J Solid State Electrochem (2005) 9: 627–633
DOI 10.1007/s10008-004-0621-y

ORIGINAL PAPER

A. Concheso · R. Santamaría · R. Menéndez
J. M. Jiménez-Mateos · R. Alcántara · P. Lavela
J. L. Tirado

Effect of oxidative stabilization on the electrochemical performance of carbon mesophases as electrode materials for lithium batteries

Received: 7 September 2004 / Revised: 26 October 2004 / Accepted: 27 October 2004 / Published online: 28 January 2005

Abstract The effect of oxidative stabilization as a mean to modify the carbon texture was essayed in a group of mesophases previous to carbonization at 900 °C with the aim of evaluating the influence on electrochemical performance when used as electrode materials in lithium test cells. X-ray diffraction, optical microscopy and chemical analysis, Fourier-transform infrared spectroscopy have been used to describe the compositional and textural properties of the as-produced parent mesophases, the samples were further treated under air current to stabilize their microstructures and the corresponding carbonized samples at 900 °C. The electrochemical performance was determined by the galvanostatic method and further correlated to the physical–chemical properties and interface resistance of the materials. In all cases, the stabilization process has demonstrated a beneficial effect on the capacity retention in the measured range.

Introduction

Much attention has been paid to new materials capable of replacing metallic lithium in advanced batteries. The need for solids that react with lithium at potentials close to that of the Li^+/Li pair has developed a wide domain of research in the last decades. Thus, formation of lithium–metal intermetallic compounds from tin composites [1], insertion in titanium spinel oxides [2], conversion reactions on transition metal oxides [3] and lithium storage in carbonaceous materials [4] have demonstrated to be successful mechanisms for reversible electrochemical reactions with lithium.

Concerning carbonaceous materials, the use of low temperature carbons in the negative electrode of Li-ion batteries has economical advantages, by allowing the reutilization of industrial waste materials or cheap by-products. Moreover, these materials usually circumvent some drawbacks arising from the use of graphitic carbons, such as exfoliation [5] and lithium metal deposition on carbon surface at cell potentials close to 0 V. Also, the highly disordered microstructure of low temperature carbons provides a number of additional surface sites, such as pores, cavities, defects, etc [6], where lithium is reversibly linked to carbon atoms even in a wider extent than in the graphene interlayer spacing. Consequently, the theoretical capacity limit set up for a graphite structure (Li_xC_6; 372 mAh/g) can be largely exceeded.

A huge variety of materials were reported so far among both soft and hard carbons arising from petroleum, carbon or other organic precursors [7–10]. Heat treatments at temperatures ranging from 600 °C to 3,000 °C provides an extra diversity of electrode materials, in which the compositional and textural properties have demonstrated to have a direct influence on their electrochemical performance when tested in lithium cells. Particular interest has been posed on anisotropic carbonaceous materials such as mesocarbon microbeads, because of their high capacities when they are carbonized at low temperatures [11, 12]. Also, chemical treatments such as mild oxidation [13] have probed to improve the electrochemical behaviour of the carbon material as electrode in lithium cell. Moreover, oxidative stabilization has been previously reported as a mean to preserve the anisotropic texture avoiding the softening process during carbonization [14].

A. Concheso · R. Santamaría · R. Menéndez
Instituto Nacional del Carbón, CSIC, Apartado 73, 33080 Oviedo, Spain

J. M. Jiménez-Mateos
REPSOL YPF. Ctra. N-V km 18, 28930 Madrid, Spain

R. Alcántara · P. Lavela (✉) · J. L. Tirado
Laboratorio de Química Inorgánica,
Universidad de Córdoba, Campus de Rabanales,
14071 Cordoba, Spain
E-mail: iq1lacap@uco.es

In this work, three mesophase samples from different origins (Petroleum, coal-tar pitch and naphthalene) were selected with the aim of elucidating the influence of both the precursor source and the stabilization treatment on the electrochemical properties in lithium test cells.

Materials and methods

Three different carbon mesophases were prepared from distinct sources. Two of them were obtained from decanted oil and coal-tar pitch, respectively. A pyrolysis treatment of the raw materials at 440 °C for 4 h led to the formation of both isotropic and anisotropic phases, which were separated by sedimentation, as described elsewhere [15]. The respective anisotropic phases deposited at the bottom of the vessel, henceforth referred to as mesophase from decanted oil (MD) and mesophase from coal-tar pitch (MP), were collected. The third carbon mesophase, was the synthetic mesophase pitch R24 (MS in this work), a commercial product from Mitshubishi Gas Chemical.

These raw mesophases were further carbonized at 900 °C for 1 h and named as MD900, MP900 and MS900, respectively. The heating ramp was set at 2 °C per min. Alternatively, the raw mesophases were submitted to an oxidative stabilization treatment at 270 °C under a high airflow rate (20 L min^{-1}) rate, previous to carbonization. These samples will be henceforth referred to as MDEST, MPEST and MSEST. The heating ramp was 1 °C/min to avoid softening and to ensure the expected oxygen–carbon reaction. The corresponding samples resulting after carbonization at 900 °C for 1 h will be henceforth referred to as MDEST900, MPEST900 and MSEST900. Finally, all samples were ground and sieved to obtain a particle size lower than 75 μm.

Carbon, hydrogen, nitrogen and sulphur contents were determined using a LECO-CHNS-932 elemental analyser, while the oxygen content was directly measured using a LECO-VTF-900 graphite furnace. FTIR spectra were registered using a Nicolet Magna IR-560 spectrometer equipped with mercury–cadmium telluride detector operating at 4 cm^{-1}. The diffusion reflectance spectra were converted to the Kubelka–Munk function. Aromaticity indices were calculated following the method described in [16].

Optical microscopy images were recorded on previously polished samples using a polarized-light microscope Zeiss Axioplan equipped with a 1-λ retarder plate. X-ray diffraction (XRD) patterns were recorded in a Siemens D-5000 equipment provided with a CuKα radiation. The interlayer distances were calculated from the (0 0 2) reflection. Crystallite size, Lc and La, were calculated from the Scherrer equation [17] with the Warren constants [18] after correction for Lorentz-polarization and instrumental broadening.

The electrochemical behaviour was evaluated using two electrodes Swagelok type cells. At one extreme, counter electrodes were 9 mm lithium metal discs and, on the other, working electrodes were made of a mixture of 92% active material and 8% PVDF binder supported on a cooper foil of the same diameter. Both electrodes were separated by Whatman glass fibre discs previously soaked in a 1 M $LiPF_6$ (EC:DEC = 1:1) electrolyte solution. The cycling tests were controlled by an Arbin potentiostat/galvanostat multichannel system. C/30 rates underwent for both charge and discharge branches. Impedance spectra were carried out in an Autolab PGSTAT12 system. An AC voltage signal of 5 mV was applied from 100 kHz to 2 mHz. The counter electrode was assembled in a three-electrode Swagelok T-type cell and then discharged to 0.002 V for successive cycles. Reference electrodes were also 9 mm lithium metal discs. A McPile (Biologic) potentiostat was used to control the cycling process by the potentiostatic methods at 10 mV/0.1 h. The discharged cells were allowed to relax in open circuit voltage for several hours before measuring.

Results and discussion

The chemical analysis of raw mesophases evidences several differences that justify the comparative study (Table 1) as they can contribute to explain the performance of the final materials in the electrodes. Important differences can be observed in the heteroatom content of the various pitches. Thus, the precursor obtained from decanted oil exhibits the highest sulphur content, while the highest nitrogen content was determined for the mesophase obtained from coal-tar pitch. These values

Table 1 Chemical composition of stabilized and untreated mesophase precursors

Precursor	Decanted oil		Pitch AR24		Coal-tar pitch	
Analysis	MD	MDEST	MS	MSEST	MP	MPEST
C (%)	92.62	89.67	94.10	86.43	93.89	90.90
H (%)	4.49	3.64	5.11	3.49	3.90	3.30
N (%)	0.35	0.37	0.03	0.03	1.20	1.30
S (%)	1.93	1.80	0.15	0.17	0.39	0.40
O (%)	0.61	4.52	0.61	9.88	0.62	4.10
C/H	1.72	2.05	1.53	2.06	2.01	2.30
C/O	202.45	26.45	205.68	11.66	201.91	29.56
I_{ar}	0.45	0.54	0.38	0.59	0.69	0.81

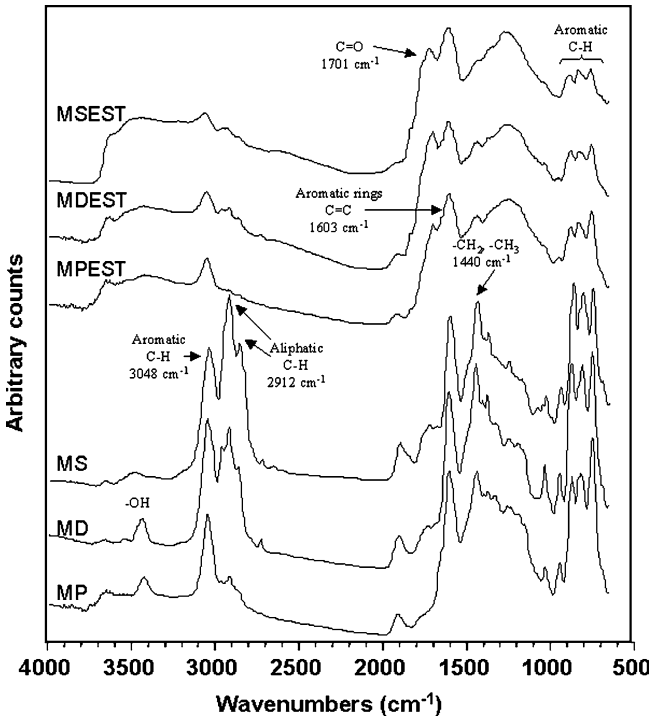

Fig. 1 FTIR spectra of stabilized (MPEST, MDEST, MSEST) and untreated (MP, MD, MS) mesophases previous to carbonization

remained almost constant after the oxidative treatment. Probably the most relevant heteroatom for this particular study is hydrogen, as it determines the reactivity of the pitch during stabilization. The highest H content is observed for MS and the lowest for MP, but not only the amount is important, but also the aliphatic/aromatic character of those H is determinant during oxidation. FTIR spectra of raw mesophases give crucial information about the functionalized groups and their further evolution upon the oxidative stabilization (Fig. 1). The two bands centred at 3,048 and 2,912 cm^{-1} are assigned to aromatic and aliphatic C–H bonds, respectively, and their intensity ratio can be used to obtain semiquantitative information represented as the aromaticity index (Table 1). MP is highly aromatic ($Iar = 0.69$), while in MS aliphatic hydrogens are more abundant ($I_{ar} = 0.38$). As it is well known, the reaction of the oxygen during stabilization occurs preferentially on the aliphatic hydrogen, so MS is the most sensitive pitch to this treatment. To support this assessment Table 1 shows the oxygen and hydrogen content of the pitches before and after the stabilization. During oxidation more than 30% of the former hydrogen of MS is depleted, to only 15% in MP and nearly 19% in MD. It can be observed in Fig. 1 that the reduction in the band centred at 2,912 cm^{-1} is larger than the reduction occurring in the band centred at 3,048 cm^{-1}. However, even more significant is the increase in the oxygen content that reaches 9.9% in MS after the stabilization, more than double than in the other two pitches. These changes are ascribable to the decomposition and removal of the smaller molecules and the promotion of the functionalization of surface sites [19]. The stabilization process also involves the increase of the C = O signal intensity at 1,701 cm^{-1} associated to aldehyde, ketones and/or carboxylic groups parallel to the increase of a broadened band at 3,600 cm^{-1} corresponding to OH in alcohols, phenols and/or adsorbed water, as can be observed in Fig. 1.

During the carbonization process, nitrogen and sulphur contents were basically preserved, while hydrogen was almost completely lost (Table 2). The highest hydrogen content after carbonization was observed for the MS900 sample, probably arising from the high content previously determined in the MS mesophase. Some oxygen previously gained during stabilization was also lost upon carbonization reaching values similar to those of the non-stabilized mesophases, even though the highest oxygen contents corresponded to stabilized MDEST and MPEST samples. The chemical changes occurring during carbonization are accompanied by structural changes that might be relevant during the electrochemical performance of the anodic materials.

The XRD patterns of carbonized samples were all characteristic of disordered carbon whose most remarkable feature is a broadened 0 0 2 reflection. The calculated interlayer spacings (Table 2) were in the range from 3.52 Å to 3.60 Å, which agree well with a non-

Table 2 Chemical composition and structural parameters of stabilized and untreated carbonized samples

Precursor	Decanted oil		Pitch AR24		Coal-tar pitch	
Analysis	MD (900)	MDEST (900)	MS (900)	MSEST (900)	MP (900)	MPEST (900)
C (%)	97.06	96.29	97.78	98.64	97.12	96.15
H (%)	0.63	0.65	1.50	0.61	0.66	0.77
N (%)	0.35	0.43	0.04	0.02	1.29	1.36
S (%)	1.50	1.66	0.15	0.21	0.39	0.39
O (%)	0.46	0.97	0.53	0.52	0.54	1.24
C/H	12.84	12.34	5.43	13.47	12.26	10.40
C/O	281.33	132.36	245.99	252.92	239.80	103.39
$d_{0\,0\,2}$(Å)	3.55	3.57	3.52	3.55	3.53	3.60
Lc (Å)	17	16	20	17	17	15
La (Å)	56	45	45	44	44	36
d_{He}(g/cm^3)	1.93	1.94	1.79	1.85	1.90	1.91

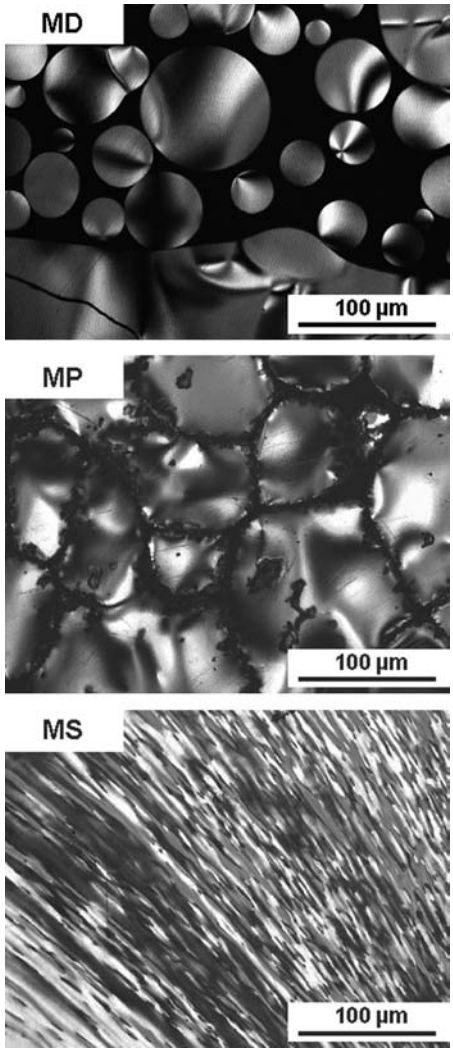

Fig. 2 Optical microscopy images of mesophase precursors MP, MD and MS samples

graphitized material. The differences between Lc and La values agree with the layered nature of the domains. Although large changes of the domain size were not detected, a decrease in these values was the general trend in stabilized carbons.

The optical images of the raw mesophases are depicted in Fig. 2. Quite different textures can be observed for each sample. Thus, the MD mesophase is characterized by well-formed domains, while MS sample shows in turn flow domains due to the extrusion step existing in their production process. In contrast, the presence of quinolein insoluble (QI) surrounding the MP spheres hinders their coalescence, maintaining the mesophase their spherical shape although deformed due to the sedimentation. The carbonization treatment at 900 °C provokes a growth of the crystalline domain and the loss of their spherical shape to become more flowed, probably caused by the softening of the carbon upon heating (Fig. 3). The primary QI are segregated from the mesophase forming clusters of the tiny particles. MS, partly due to the melting of the pitch, suffers a considerable bloating during carbonization, yielding a foam-like material with thin walls surrounding big pores. In contrast, the oxidative stabilization prevents the softening of the mesophase pitches and consequently the bloating during carbonization. The aim of this treatment is to preserve the microstructure of the material, and the achievement of this objective can be seen in Fig. 3 where the non-coalesced mesophase spheres remain as such after carbonization when stabilization is performed, with some isotropic material being maintained.

The galvanostatic charge and discharge curves are characteristic of low temperature carbons (Fig. 4). Three different zones were detectable during discharge, which are ascribable to distinct lithium reactions with carbon. A moderately steep voltage decrease is currently observed between 1.2 V and 0.8 V, which has been ascribed to different possible mechanisms, such as reversible Li–H reaction [20], solid electrolyte interface (SEI) formation [21] or lithium storage in void spaces with a high content of heteroatoms [22]. In all cases, the heteroatoms content seems to be determining for the reaction at this level. From 0.8 to 0.2, a steady decrease in cell potential is assigned to lithium insertion into the graphene layers [23]. Also, several models have been reported for lithium reaction beneath 0.2 V. The quasi-plateau observed near 0 V has been ascribed to Li^+ storage in nanopores and cavities with low content in heteroatoms [22]. The stabilization reaction involved an increase of capacity and charge/discharge reversibility for MPEST900 and MDEST900 samples. By avoiding the softening of the sample, this treatment hinders further stacking of carbon layers and assures the occurrence of edges and cavities on the carbon surface. It is corroborated by the slight increase in d_{002} interlayer spacing observed for the stabilized-carbonized samples (Table 2). These surface sites provide links for the reversible reaction of lithium. These carbons are characterized by a large number of internal surface sites where lithium can be reversibly stored [24]. The extended discharge of MS900 can be ascribed to the higher hydrogen content of this sample, which correlates well with a particularly low He density (Table 2). The quasi-reversible reaction of Li and H has demonstrated to be responsible of a high polarization between charge and discharge processes [20]. Also, the low He density measured in this sample may indicate a higher content of pores inaccessible to He where lithium can be quasi-reversibly linked, contributing to increase the capacity values close to 0 V. On the other hand, the higher contents of N and S in MD-MD900 and MP-MP900 samples, respectively, does not seem to influence so much the overall capacity and irreversibility of the first cycle as compared to hydrogen.

Further cycling confirmed these assumptions (Fig. 5). Thus, better capacity retention and higher capacity values were registered for MDEST900 and MPEST900 materials as compared with the untreated samples. The higher initial capacity of the MS900 sample progressively faded. However, the lower initial capacity of

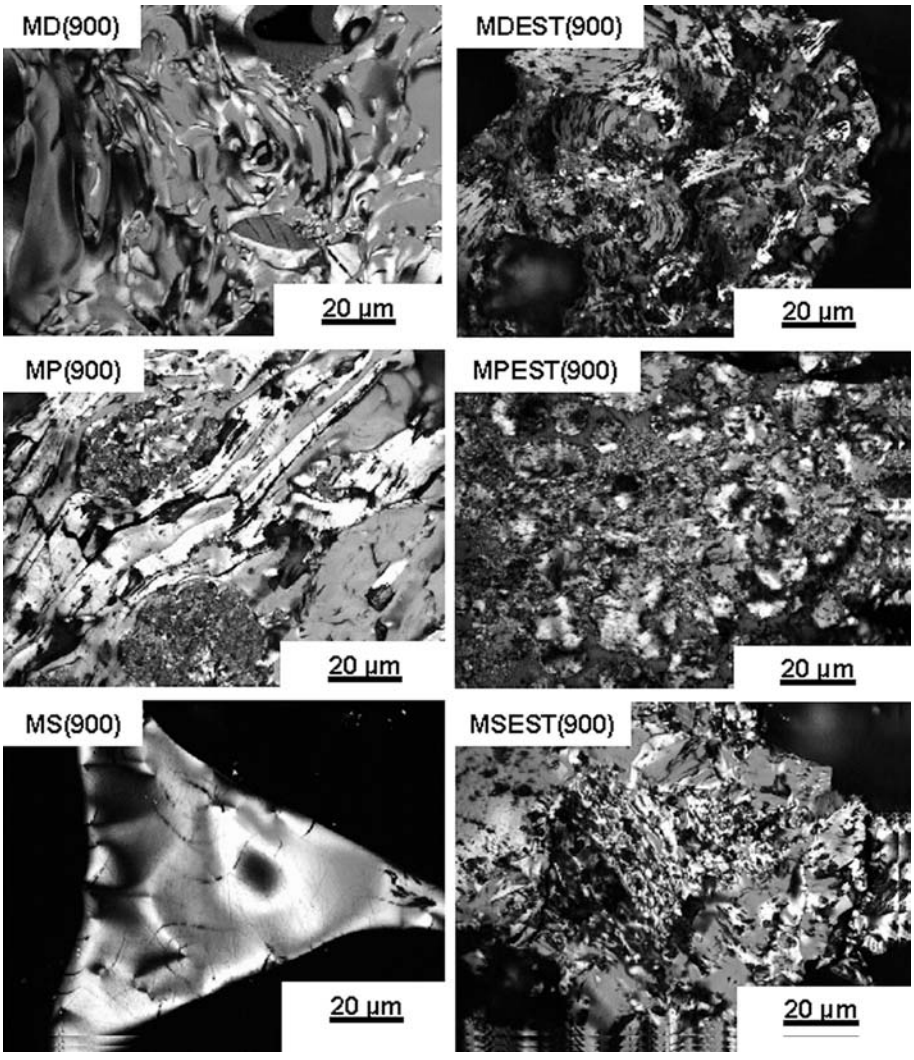

Fig. 3 Optical microscopy images of mesophases carbonized at 900 °C

MSEST900 sample was effectively maintained in the whole range of measured cycles. The MDEST900 sample reached 299 mAh/g after 19 cycles. These results evidence the beneficial effect of the oxidative stabilization process on the electrochemical performance of carbonaceous materials. The changes in texture induced in the mesophases led to an extended cycling with lower capacity losses as compared to untreated samples.

Nyquist plots of lithium test cells built up with carbonaceous materials and discharged at 0.003 V are plotted in Fig. 6. These spectra are characterized by two semicircles from high to medium frequencies whose diameters correspond to Li-ion migration through surface films that cover the active mass, and charge transfer coupled with interfacial capacitance in the interface between the carbon mass and the surface films, respectively [25, 26]. The depression of the semicircles is commonly ascribed to inhomogeneities in the electrode material such roughness, porosity and/or polycrystalline state, which hinder the frequency dispersion in the interface. Unfortunately, estimation of capacitance from the fitted parameters is considered illogical, the interfacial double layer involving CPE being a dissipative one [27]. The first large high-frequency semicircle found for all samples after stabilization could be ascribed to the deposition of a well-formed SEI. The higher complexity in the texture of stabilized samples, as observed by optical microscopy, could favour the formation of the passivating film. If we assume that the loss of oxygen in carbon can be related to the formation of a reactive surface site, the promotion of the SEI formation could arise from the strong oxygen loss observed in stabilized samples during carbonization. MP900 and MD900 samples also exhibit a net increase in the size of their medium-frequency semicircles upon the stabilization process, while MS900 reveals a decrease in the diameter of this semicircle. For the MS900 sample, the larger medium frequency semicircle, as compared to MSEST900, can be interpreted in terms of its larger domains size offering a lower number of edges and defects through which lithium could penetrate in the carbon microstructure. In the same way, the smaller and anisotropic domains observed after stabilization with air, particularly for MPEST900 and MDEST900 samples, yield a more tangled path for

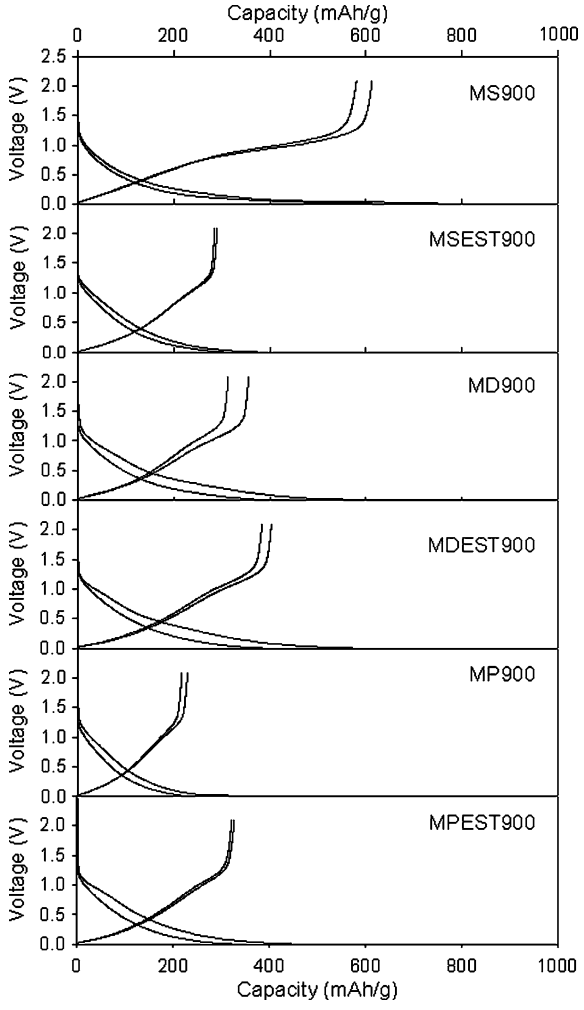

Fig. 4 Galvanostatic discharge/charge curves of mesophases carbonized at 900 °C

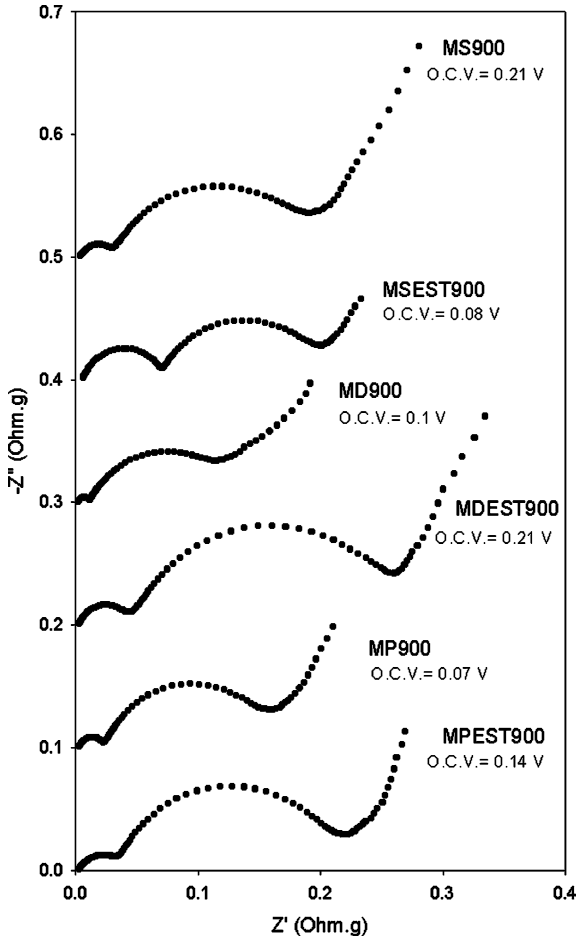

Fig. 6 Nyquist plots of mesophases carbonized at 900 °C after the first discharge

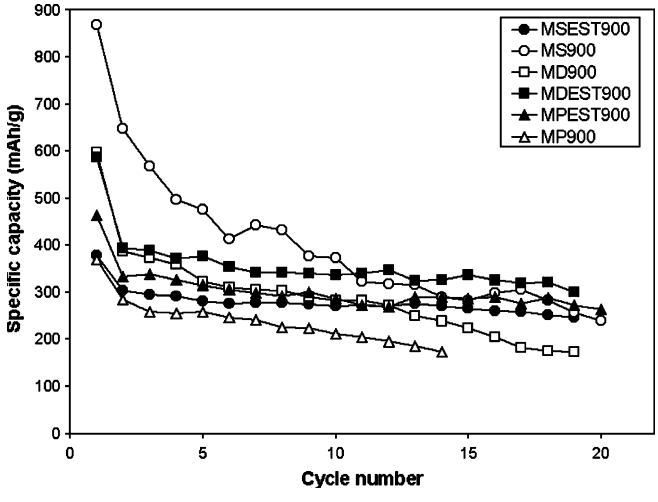

Fig. 5 Extended galvanostatic cycling of mesophases carbonized at 900 °C at C/30

lithium diffusion through the interface between the carbon mass and the surface films.

From the fit of the spectra to the equivalent circuit in Fig. 7a, charge transfer resistance values (R_3) could be calculated and plotted as a function of cycle number for the first few cycles (Fig. 7b). Upon cycling, a continuous increase in R_3 values is observed, especially for MS900. This behaviour could explain the lowest capacity retention observed for MS900. The initial differences in resistance values between stabilized and untreated carbons diminished for samples prepared from decanted oil (MD) and coal-tar pitch (MP), reaching similar values for the measured range. This more steady increase of charge transfer resistance observed for stabilized samples could be responsible of their better capacity retention. In fact, capacity tends to reach values almost constant between the first and the seventh cycle. However, it cannot be directly related to capacity fade during cells cycling for MD900 and MP900. These samples exhibited a worse retention of the discharge capacity in spite of their slightly lower R_3 values. Probably the oxidative stabilization yields a more stable microstructure by the promotion of cross-linkings between and

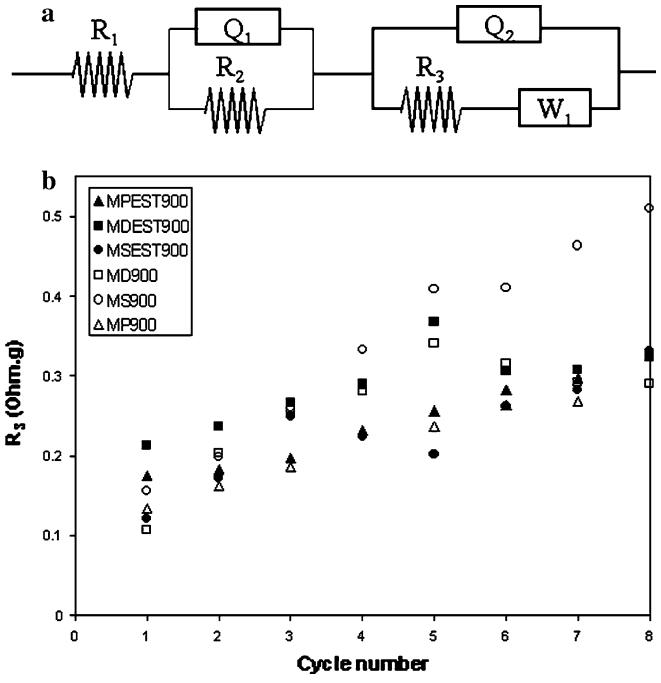

Fig. 7 **a** Analogue circuit for the fitting of the impedance response and **b** charge transfer resistance values versus cycle curves of mesophases carbonized at 900 °C

hence the structural endurance against electrochemical grinding.

Conclusions

Three mesophase samples arising from different sources have been used as precursors to prepare carbonized materials. In order to preserve the carbon texture, softening was avoided by oxidative stabilization preserving the original microtexture of the parent mesophases. Chemical analysis showed differences in hydrogen loss and oxygen gain after stabilization for the various mesophases, as expected.

Optical microscopy images allowed us to observe the different texture of both mesophase precursors and carbonized samples, showing that the stabilization process leads to smaller textures randomly oriented while non-stabilized samples, mainly MD900 and MS900, were characterized by large flowed domains.

The previous characterization has been correlated to the electrochemical performance of these carbonized materials when used as working electrodes in lithium test cells. Thus, the higher hydrogen content of sample MS900 involved a higher polarization between discharge and charge curves and higher capacity for the first cycles. However, the other samples did not exhibit significant differences among them. The most significant divergences arise from the results of cycling experiments. Thus, better capacity retention was always observed for carbonized stabilized samples as compared with the carbonized ones, with values as high as 299 mAh/g for MDEST900 after 19 cycles. This behaviour cannot be exclusively ascribed to kinetic effects on the material interfaces as has been demonstrated from impedance analysis. Most probably, the anisotropic assembly of carbon particles in stabilized samples and the promotion of cross-linkings between basic carbon units enhances the ability of these materials to endure the structural degradation usually observed during cycling.

Acknowledgements The authors are grateful to CICYT for financial support (Contract MAT2002-00434 and contract MAT2001-1694) and M.C. Mohedano for her technical support. R. Alcántara is indebted to MCYT (programa Ramón y Cajal). A. Concheso is indebted to MCYT for his predoctoral grant.

References

1. Idota Y, Kubota T, Matsufuji A, Maekawa Y, Miyasaka T (1997) Science 276:1395
2. Ohzuku T, Ueda A, Yamamoto N (1995) J Electrochem Soc 142:1431
3. Polzot P, Laruelle S, Grugeon S, Dupont L, Tarascon J-M (2000) Nature 407:496
4. Fong R, Von Sacken U, Dahn JR (1990) J Electrochemical Soc 137:2009
5. Alcántara R, Fernández Madrigal FJ, Lavela P, Tirado JL, Jiménez Mateos JM, Gómez de Salazar C, Stoyanova R, Zhecheva E (2000) Carbon 38:1031
6. Zhecheva E, Stoyanova R, Jiménez-Mateos JM, Alcántara R, Lavela P, Tirado JL (2002) Carbon 40:2301
7. Yazami R, Guérard D (1993) J Power Sources 4:39
8. Tirado JL, Alcántara R, Lavela P, Morales, Jiménez-Mateos JM (1996) Mater Sci Eng B 39:216
9. Alcántara R, Fernández Madrigal FJ, Lavela P, Tirado JL, Jiménez Mateos JM, Stoyanova R, Zhecheva E (1999) Chem Mater 11:52
10. Alcantara R, Lavela P, Ortiz GF, Tirado JL, Stoyanova R, Zhecheva E, Merino C (2004) Carbon 42(11):2153
11. Mochida I, Ku CH, Yoon SH, Korai Y (1999) Carbon 37:323
12. Kim JS (2001) J Power Sources 97–98:70
13. Wu YP, Holze RJ (2003) Solid State Eletrochem 8:73
14. Concheso A, Santamaría R, Granda M, Menéndez R, Jimenez Mateos JM, Alcantara R, Lavela P, Tirado JL (2004) Electrochim Acta (in press)
15. Mora E, Blanco C, Santamaria R, Granda M, Menendez R (2003) Carbon 41:445
16. Guillén MD, Iglesias MJ, Domínguez D, Blanco CG (1992) Energ Fuel 6:518
17. Scherrer P (1918) Bestimmung der Grösse und der inneren Struktur von Kolloidteilchen mittels Röntgenstrahlen. Göttinger Nachr Math Phys 2:98–100
18. Warren BE (1969) X-Ray diffraction. Addison-Wesley, Reading, pp 251–254
19. Blanco C, Lu S, Appleyard SP, Rand B (2003) Carbon 41:165
20. Zheng T, Xue JS, Dahn JR (1996) Chem Mater 8:389
21. Ein-Eli Y, Markovsky B, Aurbach D, Carmeli Y, Yamin H, Luski S (1994) Electrochim Acta 39:2559
22. Park CW, Yoon S, Lee SI, Oh SM (2000) Carbon 38:995
23. Stevens DA, Dahn JR (2001) J Electrochem Soc 148:A803
24. Zheng T, Xue JS, Dahn JR (1996) Chem Mater 8:389
25. Aurbach D, Gnanaraj JS, Levi MD, Levi EA, Fischer JE, Claye A (2001) J Power Sources 97–98:92
26. Alcantara R, Lavela P, Ortiz GF, Tirado JL, Menendez R, Santamaria R, Jimenez-Mateos JM (2003) Carbon 41:3003
27. Zoltowski P (1998) J Electroanal Chem 443:149